Articles

A Minimal Exonuclease Domain of WRN Forms a Hexamer on DNA and Possesses both 3′−5′ Exonuclease and 5′-Protruding Strand Endonuclease Activities[†]

Yu Xue,[‡] Glenn C. Ratcliff,[‡] Hong Wang,[‡] Paula R. Davis-Searles,[‡] Matthew D. Gray,[§] Dorothy A. Erie,[‡] and Matthew R. Redinbo*[,‡,||]

Department of Chemistry, University of North Carolina at Chapel Hill, Chapel Hill, North Carolina 27599,
Departments of Pathology and Biochemistry, University of Washington, Seattle, Washington 98195, and
Department of Biochemistry and Biophysics and Lineberger Comprehensive Cancer Center,
University of North Carolina at Chapel Hill, Chapel Hill, North Carolina 27599

Received August 23, 2001; Revised Manuscript Received January 14, 2002

ABSTRACT: Werner syndrome is a rare autosomal recessive disease characterized by a premature aging phenotype, genomic instability, and a dramatically increased incidence of cancer and heart disease. Mutations in a single gene encoding a 1432-amino acid helicase/exonuclease (hWRN) have been shown to be responsible for the development of this disease. We have cloned, overexpressed, and purified a minimal, 171-amino acid fragment of hWRN that functions as an exonuclease. This fragment, encompassing residues 70−240 of hWRN (hWRN-N_{70-240}), exhibits the same level of 3′−5′ exonuclease activity as the previously described exonuclease fragment encompassing residues 1−333 of the full-length protein. The fragment also contains a 5′-protruding DNA strand endonuclease activity at a single-strand−double-strand DNA junction and within single-stranded DNA, as well as a 3′−5′ exonuclease activity on single-stranded DNA. We find hWRN-N_{70-240} is in a trimer−hexamer equilibrium in the absence of DNA when examined by gel filtration chromatography and atomic force microscopy. Upon addition of DNA substrate, hWRN-N_{70-240} forms a hexamer and interacts with the recessed 3′-end of the DNA. Moreover, we find that the interaction of hWRN-N_{70-240} with the replication protein PCNA also causes this minimal, 171-amino acid exonuclease region to form a hexamer. Thus, the active form of this minimal exonuclease fragment of human WRN appears to be a hexamer. The implications these results have on our understanding of hWRN's roles in DNA replication and repair are discussed.

Werner syndrome (WS)[1] is an autosomal recessive disease characterized by the early onset of an aged appearance along with the common disorders associated with advancing age

(*1, 2*). These disorders include atherosclerosis, bilateral cataracts, diabetes mellitus, and osteoporosis, as well as an unusually high incidence of tumors of non-epithelial cell origin. WS cells are characterized by chromosomal translocations, defective maintenance of telomeres, elevated rates of homologous recombination, large DNA deletions, and a prolonged S-phase of DNA synthesis (*3−10*). *WRN*, the gene defective in WS, consists of 35 exons that encode a 1432-amino acid protein (hWRN). This protein functions both as a 3′−5′ DNA helicase and as a 3′−5′ exonuclease (*6, 11−13*). In addition, one group has reported that hWRN is also a 5′−3′ exonuclease (*14*). The sequence of the helicase domain is homologous to members of the RecQ family of DNA helicases (*15*). This family includes *Escherichia coli* RecQ, *Saccharomyces cerevisiae* Sgs-1p, *Schizosaccharomyces pombe* Rqh-1p, human RecQL, and the protein associated with Bloom syndrome, BLM (*16−20*). Of the RecQ helicases identified so far, only the WRN protein functions both as a helicase and as an exonuclease. How these two functions are coupled during DNA metabolic events in vivo remains unclear.

Table 1: DNA Molecules Employed in These Studies

length	sequence
substrate R	
24 nucleotides	5′-d(CAGGCACAGGGTCAGGTCGGGGGG)-3′
60 nucleotides	5′-d(TCTACGCTCTGAGTGACTGACAAGTTTTTTTTTTTTCCCCCCGACCTGACCCTGTGCCTG)-3′
substrate S	
20 nucleotides	5′-d(CGCTAGCAATATTCTGCAGC)-3′
46 nucleotides	5′-d(GCGCGGAAGCTTGGCTGCAGAATATTGCTAGCGGGAAATCGGCGCG)-3′
substrate L	
1 kb DNA duplex with a 100-base 5′-overhang	

The conserved exonuclease motif of WRN is located in the N-terminus, while the RecQ helicase motif is more centrally located with respect to the N- and C-termini. It has been shown that hWRN can efficiently degrade 3′-recessed DNA strands of double-stranded or DNA–RNA heteroduplexes (*12*, *13*). hWRN has little activity on blunt-ended DNA, on DNA with a 3′-protruding strand, or on single-stranded DNA (*5*). In the presence of the Ku 70/80 heterodimer, however, the exonuclease activity of hWRN is altered. For example, hWRN is stimulated to degrade blunt-ended and single-stranded DNA substrates in a 3′–5′ direction in the presence of Ku (*21*, *22*, *49*, *50*). The interaction of hWRN with the Ku heterodimer is mediated by residues 1–50 of hWRN (*50*).

Information obtained from protein sequence database searches revealed that the exonuclease domain of hWRN is contained within the first 333 amino acids at the N-terminus (*5*). This region is significantly similar to the 3′–5′ proofreading domain of *E. coli* polymerase I, RNAseD, and the nuclease domain of the human polymyositis/scleroderma nuclear autoantigen (*23*). Within this N-terminal exonuclease region, five amino acids (Asp82, Glu84, Asp143, Tyr212, and Asp216) are proposed to be critical for exonuclease activity (*5*).

The biological function of the WRN helicase/exonuclease is unclear. It is possible that WRN participates in one or more aspects of DNA replication because abnormalities in both S-phase initiation and transition have been reported in cells harboring WRN mutations (*5*, *24*). Its efficient removal of terminally mismatched nucleotides raises the possibility that WRN may provide a 3′–5′ proofreading activity for DNA polymerases that lack such an activity (*25*). The findings that WRN interacts with numerous proteins involved in DNA replication, recombination, and repair, including PCNA (*5*, *26*), Ku (*21*, *22*, *49*, *50*), p53 (*27*), RPA (*28*, *29*), and DNA Pol δ and topoisomerase I (*30–33*), support the involvement of WRN in these processes, as well.

To gain a better understanding of the functions of the WRN exonuclease, we have performed a detailed analysis of the physical and biochemical properties of a minimal fragment comprising amino acids 70–240 at the N-terminus of hWRN (hWRN-N$_{70-240}$). We show, through a variety of techniques, that (1) hWRN-N$_{70-240}$ is capable of hydrolyzing double-stranded DNA with a 3′-recessed end in a 3′–5′ direction, (2) hWRN-N$_{70-240}$ exhibits a 5′-protruding strand endonuclease activity and a 3′–5′ exonuclease activity on single-stranded DNA, (3) hWRN-N$_{70-240}$ is in a trimer–hexamer equilibrium in the absence of substrate, (4) hWRN-N$_{70-240}$ forms a hexamer on a DNA substrate containing a recessed 3′-end, and (5) the interaction of hWRN-N$_{70-240}$

with PCNA causes hWRN-N$_{70-240}$ to form a hexamer. These results indicate that this minimal exonuclease region of hWRN is active as a hexamer and is capable of functioning both as an exonuclease and an endonuclease. The implications these results have on our understanding of the nuclease functions of full-length WRN are discussed.

MATERIALS AND METHODS

Materials

The expression vector pET15b and BL21(DE3) cells were obtained from Stratagene. The Ni–NTA resin was from Qiagen. Superdex 200 resin was purchased from Bio-Rad and DEAE-Sepharose from Pharmacia. [γ-^{32}P]ATP was obtained from NEN Life Science Products. Bacteriophage T4 polynucleotide kinase was supplied by New England Biolabs. Deoxyribonucleoside triphosphates were purchased from Promega, and ribonucleoside triphosphates (NTPs) were supplied by GibcoBRL. Oligonucleotides (Table 1), purchased in-house (University of North Carolina at Chapel Hill), were purified by HPLC. The full-length human WRN cDNA was a gift of M. Gray and G. Martin of the University of Washington (Seattle, WA). AFM tips were purchased from Molecular Imaging, Inc. (Phoenix, AZ).

Purification of hWRN-N$_{70-240}$

hWRN-N$_{70-240}$ and hWRN-N$_{1-333}$ codons were amplified by polymerase chain reaction (PCR) and cloned into the pET15b expression vector to generate pET15b-hWRN-N$_{70-240}$ and pET15b-hWRN-N$_{1-333}$. The point mutation E84A (Glu → Ala at amino acid 84) was introduced by site-directed PCR mutagenesis to generate pET15-hWRN-N$_{70-240}$E84A. The cloned hWRN sequence, exonuclease mutation, and cloning in frame to the hexahistidine tag in the expression vectors were verified by DNA sequencing. Recombinant proteins were produced according to the supplier's protocol. Cells were lysed in 20 mM Tris-HCl (pH 7.8), 300 mM NaCl, 5% glycerol, 1 mM phenylmethanesulfonyl fluoride (PMSF), and 1 mM β-ME and disrupted with a sonicator. The lysate was clarified by centrifugation and incubated with Ni–NTA resin at 4 °C for 1 h. The resin was then washed with 20 mM Tris-HCl (pH 7.8), 300 mM NaCl, and 5% glycerol, and protein was eluted with 20 mM Tris-HCl (pH 7.8), 300 mM NaCl, 5% glycerol, and 250 mM imidazole. DTT (20 mM) was added to the eluted protein. The protein sample was heated at 37 °C for 15 min with 100 mM DTT addition and loaded onto a Superdex S-200 column (80 cm), which was previously equilibrated in buffer A [20 mM Tris-HCl (pH 7.8), 30 mM NaCl, and 5% glycerol]. Pooled fractions of hWRN-N$_{70-240}$ from Superdex S-200 were finally

```
human_WRN_1-360     1 MSEKKLETTAQQRKCPEWMNVQNKRCAVEERKACVRKSVFEDDLPFLEFT

mouse_WRN_1-360     1 -----METTSLQRKFPEWMSMQSQRCATEEK-ACVQKSVLEDNLPFLEFP


human_WRN_1-360    51 GSIVYSYDASDCSFLSEDISMSLSDGDVVGFDMEWPPLYNRGKLGKVALI

mouse_WRN_1-360    45 GSIVYSYEASDCSFLSEDISMRLSDGDVVGFDMEWPPIYKPGKRSRVAVI


human_WRN_1-360   101 QLCVSESKCYLFHVSSMSVFPQGLKMLLENKAVKKAGVGIEGDQWKLLRD

mouse_WRN_1-360    95 QLCVSESKCYLFHISSMSVFPQGLKMLLENKSIKKAGVGIEGDQWKLLRD


human_WRN_1-360   151 FDIKLKNFVELTDVANKKLKCTETWSLNSLVKHLLGKQLLKDKSIRCSNW

mouse_WRN_1-360   145 FDVKLESFVELTDVANEKLKCAETWSLNGLVKHVLGKQLLKDKSIRCSNW


human_WRN_1-360   201 SKFPLTEDQKLYAATDAYAGFIIYRNLEILDDTVQRFAINKEEEILLSDM

mouse_WRN_1-360   195 SNFPLTEDQKLYAATDAYAGLIIYQKLGNLGDTAQVFALNKAEENLPLEM


human_WRN_1-360   251 NKQLTSISEEVMDLAKHLPHAFSKLENPRRVSILLKDISENLYSLRRMII

mouse_WRN_1-360   245 KKQLNSISEEMRDLANRFPVTCRNLETLQRVPVILKSISENLCSLRKVIC


human_WRN_1-360   301 GSTNIETELRPSNNLNLLSFEDSTTGGVQQKQIREHEVLIHVEDETWDPT

mouse_WRN_1-360   295 GPTNTE--------------------------------------------


human_WRN_1-360   351 LDHLAKHDGE

mouse_WRN_1-360       ----------
```

FIGURE 1: Amino acid sequence alignment of residues 1−360 from the N-terminal regions of the human and mouse WRN proteins, generated using Workbench software. Identical amino acids are in red; similar amino acids are in blue, and the five amino acids thought to be critical for exonuclease activity are bold.

subjected to anion exchange chromatography (Q-Sepharose fast flow). The column was pre-equilibrated in buffer A before loading the protein. After the column had been washed with 1 column volume of equilibration buffer, proteins were eluted by successive washes with three to four column volumes with each portion of buffer A containing 50, 100, 150, and 200 mM NaCl. SDS−PAGE resolution followed by Coomassie Blue staining of proteins indicated that the major protein of the ∼22 kDa hWRN-N$_{70-240}$ protein was present in the 150 mM NaCl eluate. Pooled hWRN-N$_{70-240}$ fractions with a typical total protein content of 5−7 mg were concentrated to 10 mg/mL in the same buffer. The concentrated hWRN-N$_{70-240}$ proteins were resolved by SDS−PAGE and assayed for DNA exonuclease activity. The activity remained stable for at least 1 month at −80 °C. Protein concentrations were determined by the Bradford assay. hWRN-N$_{1-333}$ and hWRN−N$_{70-240}$E84A were purified in a fashion identical to that used for hWRN-N$_{70-240}$.

DNA Labeling and Annealing

Single-stranded DNA oligomers were labeled with ^{32}P at their 5′-ends as described in Molecular Cloning (*34*). To form the partial DNA duplex for exonuclease activity assay, the labeled oligomer was mixed with the complementary unlabeled DNA oligomer (1:1) in 50 mM Tris-HCl (pH 7.8) and 5 mM MgCl$_2$. The DNA mixture was heated to 100 °C for 10 min and then allowed to anneal slowly by cooling to room temperature overnight. The resulting partial duplex containing a 3′-recessed terminus was ethanol-precipitated two times and resuspended in 100 μL of ddH$_2$O.

Assays for WRN Nuclease Activities

^{32}P-labeled DNA substrate (0.1 pmol) was incubated with 25 fmol of recombinant hWRN-N$_{70-240}$ at 37 °C in a 10 μL reaction mixture containing 40 mM Tris-HCl (pH 7.4), 4 mM MgCl$_2$, 5 mM DTT, 100 μg/mL BSA, and 1 mM ATP. The protein was incubated with DNA for increasing lengths of time, and DNA hydrolysis was terminated by addition of quench buffer (0.5 mM EDTA and 80% formamide). At the indicated time points (e.g., in Figure 2B, 0, 1, 2, 5, 10, 15, 20, 30, and 40 min), 4 μL of quench buffer was added to 8 μL of the reaction mixture. An aliquot of 6 μL of denaturing loading buffer (76% formamide, 20 mM EDTA, 2% SDS, 3% bromophenol blue, and 3% xylene cyanol) was added
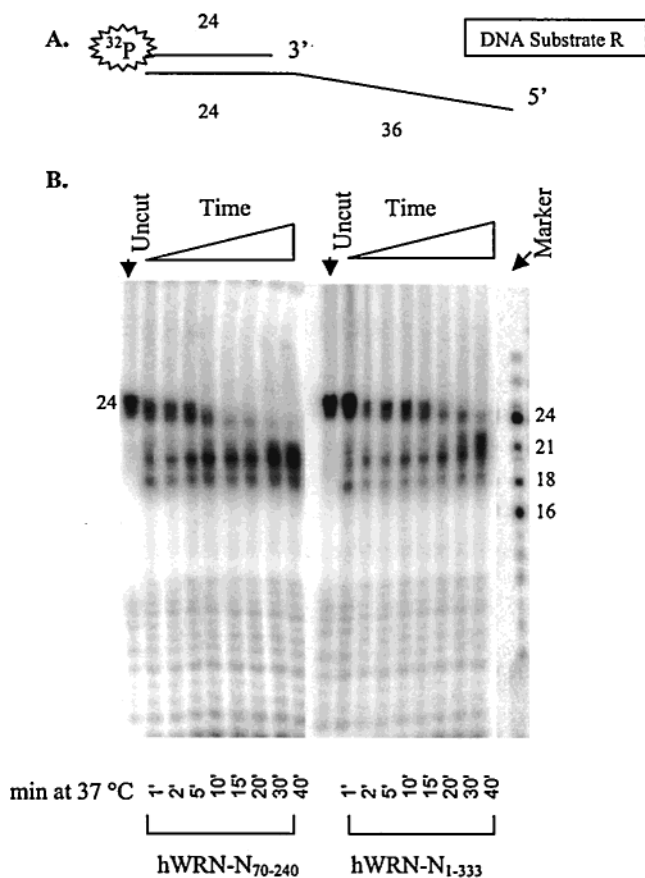
A.

B.

FIGURE 2: (A) DNA duplex (substrate R) composed of a ^{32}P-5′-labeled (star) 24-mer with a recessed 3′-end and an unlabeled 60-mer (see Table 1). (B) hWRN-N$_{70-240}$ and hWRN-N$_{1-333}$ exonuclease activities on a DNA substrate with a recessed 3′-end. The lane marked "uncut" contains DNA that has not been treated with either hWRN-N$_{70-240}$ or hWRN-N$_{1-333}$. The times below each lane correspond to the length of time DNA substrate R was incubated with an hWRN-N construct at 37 °C prior to the addition of 0.5 mM EDTA and 80% formamide. The nucleolytically fragmented ^{32}P-5′-labeled 24-mer was resolved from undigested DNA by electrophoresis through a 20% denaturing polyacrylamide gel as described (see Materials and Methods).

to 6 μL of the stopped reaction mixture. The mixture was heated at 100 °C for 1 min prior to electrophoresis on an 8 M urea/20% polyacrylamide gel in 1× TBE (90 mM Tris base, 90 mM boric acid, and 1 mM EDTA). Gels were vacuum-dried, and reaction products were visualized by autoradiography and quantified with a PhosphoImager (Molecular Dynamics, Amersham Pharmacia Biotech, Piscataway, NJ). Assays involving hWRN-N$_{1-333}$ and hWRN-N$_{70-240}$E84A were performed in a manner identical to that described for hWRN-N$_{70-240}$.

Determination of Oligomerization State of hWRN-N$_{70-240}$

Ni−NTA affinity purified hWRN-N$_{70-24}$ (100 μg/100 μL) was treated with 50 mM EDTA and 100 mM DTT for 15 min at 37 °C and then subjected to gel filtration at 4 °C. The column was a Superdex S-200 column (80 cm); the flow rate was 0.5 mL/min, and the fraction size was 2 mL. Protein was eluted with 20 mM Tris-HCl (pH 7.8), 30 mM NaCl, and 0.1 mM PMSF. The column was calibrated using ferritin (440 kDa), aldolase (158 kDa), ovalbumin (43 kDa), and ribonuclease A (13.7 kDa). The elution profiles of WRN were examined by SDS−PAGE.

Atomic Force Microscopy

Protein and DNA Preparation. The imaged DNA was prepared using standard PCR techniques. The DNA that was used was a 1000 bp segment that was PCR amplified from M13 phage DNA and digested by *Bam*HI and *Ban*II restriction enzymes (named the L substrate; Table 1). Digested fragments were isolated from 0.8% agarose gels utilizing the Qiagen gel extraction kit, and then a 100 bp fragment was ligated into the end digested with *Ban*II. Yeast proliferating cell nuclear antigen (yPCNA) was a gift from T. Kunkel of the National Institute of Environmental Health Sciences (NIEHS, Research Triangle Park, NC). hWRN-N$_{70-240}$ was prepared as described above.

Imaging by Atomic Force Microscopy (AFM). Imaging was performed with a Nanoscope IIIa instrument (Digital Instrument, Santa Barbara, CA) using the tapping mode in air. Nanosensor Pointprobe noncontact/tapping mode sensors with spring constants of 48 N/m and resonance frequencies of 190 kHz were used for all images. The protein and DNA molecules were deposited onto freshly cleaved mica (Spruce Pine Mica Co., Spruce Pine, NC), washed with deionized distilled water, and dried with a stream of N$_2$ (gas). To obtain the proper surface coverage, the deposition time was varied from 5 to 60 s depending on the protein and DNA concentrations. All images were collected at a scan rate of 3.0 Hz and a scan size of 1 μm. Volume analysis using AFM data was performed using image plane fitting, image analysis, and volume calculation, as described previously (*35*).

hWRN-N$_{70-240}$−yPCNA Binding Reactions. Binding reaction mixtures included 100 nM hWRN-N$_{70-240}$, 400 nM yPCNA, 20 mM Tris-HCl (pH 7.8), 30 mM NaCl, 1 mM ATP, 5 mM MgCl$_2$, and 5% glycerol in 20 μL. After incubation for 15 min at room temperature, the reaction mixtures were diluted to 200 μL with binding buffer [20 mM Tris-HCl (pH 7.8), 30 mM NaCl, 5 mM MgCl$_2$, and 5% glycerol] and 20 μL was immediately deposited onto freshly cleaved mica.

hWRN-N$_{70-240}$−DNA Binding Reactions. Two substrates were used in the binding reactions. One is a short piece of DNA named substrate S with a top strand of 20 nucleotides and a bottom strand of 46 nucleotides (see Table 1); the other is substrate L, which contains a 100-base 5′-overhang as described above. Binding reaction mixtures included 3−4 nM DNA fragment, 400−500 nM hWRN-N$_{70-240}$, 20 mM Tris-HCl (pH 7.8), 30 mM NaCl, 5 mM MgCl$_2$, and 5% glycerol in 20 μL. After incubation for 15−20 min at room temperature, the reaction mixtures were diluted to 200 μL in binding buffer [20 mM Tris-HCl (pH 7.8), 30 mM NaCl, 5 mM MgCl$_2$, and 5% glycerol] and 20 μL was immediately deposited onto freshly cleaved mica.

Volume Calculations. The measured AFM volumes, calculated using the equation $V_i = A_i(M_i - S)$, of each of the proteins were distributed in a Gaussian fashion (*35*). The volume and its uncertainty for a given protein were taken to be the average and standard deviation of the distribution, respectively. The area A_i, total average height M_i, and surface heights are measured using ImageSXM software. Prior to volume analysis, the deposition time that produced optimal surface coverage was determined. The data were filtered to remove false positives of oligomers using major:major axis ratio cutoff values ranging from 2.0 to 2.5. Histogram plots

of the volume of the proteins were generated for each cutoff value.

RESULTS

Cloning, Expression, and Purification of hWRN-N$_{70-240}$ and hWRN-N$_{1-333}$. The hWRN exonuclease activity resides within the first 333 amino acids at the N-terminus of the protein (*5*). In aligning the hWRN and mouse WRN sequences (mWRN), we found that the region between amino acids 70 and 240 (Figure 1) exhibits 83% amino acid identity and includes all five amino acids (Asp82, Glu84, Asp143, Tyr212, and Asp216) predicted to be critical for hWRN exonuclease activity (*5*). To determine if this region of hWRN was sufficient to function as an exonuclease, we cloned, expressed, and characterized a minimal fragment of the WRN exonuclease comprised of residues 70−240 and analyzed it relative to the N-terminal 333-amino acid exonuclease fragment of WRN described previously (*5*).

Regions of the hWRN cDNA encoding amino acids 70−240 and 1−333 were amplified by the polymerase chain reaction (PCR) and cloned into pET15b to generate pET15b-hN$_{1-333}$ and pET15b-hN$_{70-240}$. In addition, the point mutation E84A (Glu to Ala at amino acid 84), previously shown to inactivate the exonuclease activity of full-length hWRN (*5*), was introduced by site-directed PCR mutagenesis to generate pET15b-hN$_{70-240}$E84A. The cloned hWRN-N$_{70-240}$, hWRN-N$_{1-333}$, and hWRN-N$_{70-240}$E84A regions were confirmed by DNA sequencing and inserted in-frame to allow the production of hexahistidine-tagged proteins.

The recombinant hWRN-N$_{1-333}$ and hWRN-N$_{70-240}$ proteins were expressed in BL21(DE3) pLys cells, and purified by Ni affinity batch preparation, gel filtration chromatography using a Superdex S-200 column, and, finally, Q-Sepharose fast flow. At the gel filtration step, the recombinant hWRN proteins eluted as a trimer as judged by the apparent molecular mass, and were found to be ∼80% pure by SDS−PAGE. After anion exchange chromatography, proteins were estimated to be >95% pure based on Coomassie blue-stained SDS−PAGE. Purified hWRN-N$_{70-240}$ had an apparent monomeric molecular mass of 21 kDa, as expected from the calculated molecular mass with the additional N-terminal 20 amino acids encoded by the hexahistidine tag and vector. Purified hWRN-N$_{1-333}$ and hWRN-N$_{70-240}$E84A had apparent molecular masses of 40 and 21 kDa, respectively.

hWRN-N$_{70-240}$ Is a 3′−5′ Exonuclease. We assayed the exonuclease activity of hWRN-N$_{70-240}$ using a 5′-labeled, 3′-recessed double-stranded DNA substrate composed of a 24-nucleotide top strand and a 60-nucleotide bottom strand which we will call substrate R (see Table 1 and Figure 2A). As shown in Figure 2, hWRN-N$_{70-240}$ and hWRN-N$_{1-333}$ both catalyze the exonucleolytic hydrolysis of the 3′-recessed end of this double-stranded DNA duplex in a 3′−5′ direction. Cleavage of the substrate radiolabeled at the 5′-terminus yields time-dependent accumulation of shorter products. In our hands, both hWRN-N$_{70-240}$ and hWRN-N$_{1-333}$ function as relatively nonprocessive 3′−5′ exonucleases. In particular, hWRN-N$_{70-240}$ appears to degrade DNA substrate R efficiently through the G$_6$ region (see Table 1) but not beyond that. No detectable hWRN-N$_{70-240}$ nuclease activity was observed using the hWRN-N$_{70-240}$E84A construct of human

WRN. Similarly, no hWRN-N$_{70-240}$ nuclease activity was observed with single-stranded DNA alone (i.e., not an overhang from a DNA duplex), blunt-ended DNA, or a DNA duplex containing a 5′-rececced end (data not shown). These results suggest that hWRN-N$_{70-240}$ exonuclease is distinguished from the large majority of the known nucleases by its preference for 3′-recessed DNA in a partial duplex.

hWRN-N$_{70-240}$ Appears To Be Trimeric As Determined by Gel Filtration Chromatography. Once we established that the minimal region of amino acids 70−240 of hWRN functioned as an exonuclease, we next sought to characterize the oligomeric state of this fragment in vitro. The fragment of residues 1−333 of hWRN was previously reported to be a trimer based on gel filtration chromatography (*5*). To determine the oligomeric structure of hWRN-N$_{70-240}$, we also employed gel filtration chromatography. Purified hWRN-N$_{70-240}$ was reapplied to the Superdex S-200 column used for protein purification (Figure 3A). A set of standard proteins was also assayed in separate runs on the same gel filtration column (see Materials and Methods), and their elution volumes were used to construct a standard curve. The hWRN-N$_{70-240}$ was found to elute in a peak corresponding to a molecular mass of 65 kDa (Figure 3A,B). As the molecular mass of the recombinant hWRN-N$_{70-240}$ is ∼21 kDa, the oligomerization state of this population of the protein appears to be trimeric.

hWRN-N$_{70-240}$ Is in a Trimer−Hexamer Equilibrium As Determined by AFM. Atomic force microscopy (AFM) can be used to image soft samples with nanometer resolution both in air and in solution (*35*). We used it to quantify intermolecular protein and protein−DNA interactions. Because AFM produces topographical images, it is possible to relate the molecular mass of a protein to its volume. Previous studies have shown a linear relationship between the measured AFM volume and the molecular mass of the proteins with the equation $v = (1.3\text{MW}) - 25$, where v is the volume measured by AFM and MW is the molecular mass (*35*). Furthermore, the expected AFM volume of oligomeric protein complexes can be predicted using this equation. Table 2 shows the possible hWRN-N$_{70-240}$ complexes considered in this study.

To determine the oligomerization state of this minimal exonuclease fragment of human WRN, hWRN-N$_{70-240}$, it was deposited at 20 nM, images were collected, and volume analysis was performed for each set of images. Figure 4A shows an ideal hWRN-N$_{70-240}$ surface coverage for volume analysis. In all, 1135 protein data points were analyzed, and a histogram of molecular volumes for hWRN-N$_{70-240}$ is shown in Figure 4B. The distribution has a major peak at ∼68 nm^3 with a shoulder at higher volumes. The major peak was fit to a Gaussian function to determine the volume. The observed AFM volume is 68 ± 8 nm^3, which corresponds to a molecular mass of 66 kDa. This mass is consistent with a trimer of hWRN-N$_{70-240}$ (see Table 2). The small peak at ∼140 nm^3 is consistent with the molecular mass of the hWRN-N$_{70-240}$ hexamer (125 kDa). Approximately 10% of the hWRN-N$_{70-240}$ is in the higher association state (hexamer). This result is consistent with the previous report that 90% of wild-type hWRN existed as trimer in the absence of DNA (*5*).

hWRN-N$_{70-240}$ Interacts with Trimeric PCNA as a Trimer and a Hexamer. Human PCNA, which is a major component
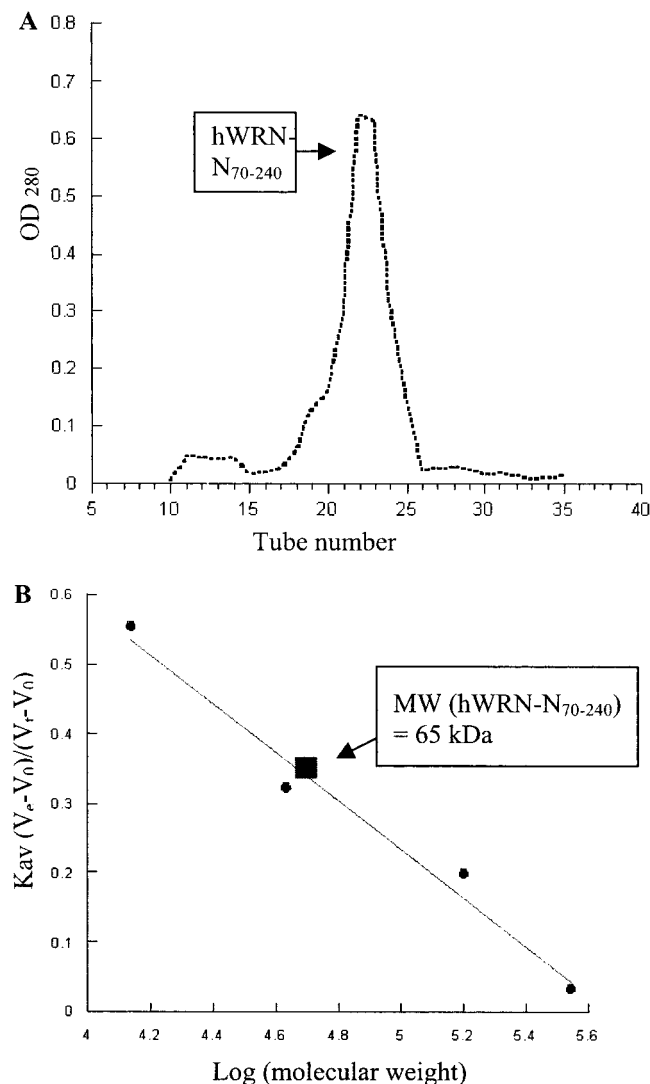
A

B

FIGURE 3: Analysis of the quaternary structure of hWRN-N$_{70-240}$ by gel filtration chromatography. (A) Elution profile for purified hWRN-N$_{70-240}$ on a Superdex S-200 column. (B) Elution of the hWRN-N$_{70-240}$ oligomers and molecular mass markers from Superdex S-200 chromatography. The molecular mass markers are ferritin (440 kDa), aldolase (158 kDa), ovalbumin (43 kDa), and ribonuclease A (13.7 kDa). The elution peak for dextran from the column was considered the exclusion volume (V_0). V_t was determined by the elution of salt from the column. V_e is the elution volume of hWRN-N$_{70-240}$ oligomers (■) and molecular mass markers (●).

of the DNA replication fork, has been reported to interact with hWRN (*5, 26*). To determine if PCNA interacts with the minimal WRN fragment hWRN-N$_{70-240}$, we imaged *S. cerevisiae* PCNA (yPCNA) alone and in complex with hWRN-N$_{70-240}$ by AFM. *S. cerevisiae* PCNA was used because a pure sample was kindly provided by T. Kunkel (NIEHS). The sequences of human and yPCNA are 35% identical, and the three-dimensional structures of these two trimeric proteins are highly similar (*36*). We used AFM to determine the oligomerization state of yPCNA and yPCNA in complex with hWRN-N$_{70-240}$. As expected, yPCNA exists as a trimer with a molecular mass of ∼92 kDa (Figure 5A). Inspection of Figure 5A reveals a single peak at ∼90 nm^3. With hWRN-N$_{70-240}$ and yPCNA together, two distinct peaks are observed at 150 and 235 nm^3 (Figure 5B). These peaks correspond to molecular masses of 135 and 200 kDa,

Table 2: Predicted and Observed AFM Volumes for hWRN-N$_{70-240}$ and PCNA Oligomers

complex	molecular mass (kDa)	predicted AFM volume (nm^3)	observed AFM volume (nm^3)
monomer hWRN-N$_{70-240}$	21	2.3	not observed
dimer hWRN-N$_{70-240}$	42	29.6	not observed
trimer hWRN-N$_{70-240}$	63	56.9	68 ± 8
hexamer hWRN-N$_{70-240}$	126	138.8	135 ± 7
monomer PCNA	29	12.7	not observed
trimer PCNA	87	88.1	94 ± 7
hexamer PCNA	174	201.2	not observed
trimer hWRN-N$_{70-240}$−trimer PCNA complex	150	170	150 ± 15
hexamer hWRN-N$_{70-240}$−trimer PCNA complex	213	251.9	235 ± 11
hexamer hWRN-N$_{70-240}$−hexamer PCNA complex	300	365	not observed

respectively. On the basis of Table 2, the first peak (135 kDa) can be explained by two species. One is a complex of a trimer yPCNA and a trimer hWRN-N$_{70-240}$ (150 kDa); the other one is a hexamer of hWRN-N$_{70-240}$ (126 kDa). However, as shown above by two methods, hWRN-N$_{70-240}$ is a trimer in the absence of DNA (Figures 3 and 4). In addition, the disappearance of the peak corresponding to the trimer of PCNA from Figure 5B provides strong evidence that the two peaks present in this figure contain PCNA and hWRN-N$_{70-240}$. Thus, we conclude that the first peak represents trimer PCNA−trimer hWRN-N$_{70-240}$ complexes. The second peak (200 kDa) can be explained by trimer yPCNA−hexamer hWRN-N$_{70-240}$ complexes (213 kDa), or by hexamer yPCNA−trimer hWRN-N$_{70-240}$ complexes (237 kDa). Because there is no evidence for PCNA hexamer formation, we conclude that the second peak is generated by complexes of yPCNA trimers and hWRN-N$_{70-240}$ hexamers. Thus, yPCNA and hWRN-N$_{70-240}$ form both trimer−trimer and trimer−hexamer complexes. Further, the interaction of PCNA with hWRN-N$_{70-240}$ appears to drive the formation of hWRN-N$_{70-240}$ hexamers.

hWRN-N$_{70-240}$ Hexamerizes on DNA. In several previous studies, AFM was used for qualitative analyses of protein−DNA complexes, including that of Cro protein, RNA polymerase, and heat shock transcription factor-2 with double-stranded DNA, and the interaction of single-stranded DNA-binding proteins and single-stranded DNA (*37−40*). These successful applications of AFM have made it possible to extend the use of AFM to the quantitative analysis of DNA−protein interactions. To test whether hWRN-N$_{70-240}$ exists as a trimer or as a higher-order oligomer in the presence of DNA, AFM images were obtained in the presence of substrate S, a 3′-recessed double-stranded DNA molecule composed of a 20-nucleotide top strand and a 46-nucleotide bottom strand (Table 1 and Figure 6A). This DNA substrate is too small, with a maximal expected length of 7 nm, to be visualized by AFM. A statistical analysis reveals that the volume distribution of hWRN-N$_{70-240}$ molecules on DNA substrate S is best explained by the existence of two populations of hWRN-N$_{70-240}$ molecules with two different sizes (Figure 6B): 45% as 60 nm^3 and 49% as 135 nm^3. On the basis of the volumes in Table 2, the smaller and larger populations are considered to be trimers and hexamers, respectively. In the absence of DNA, this hexamer peak is
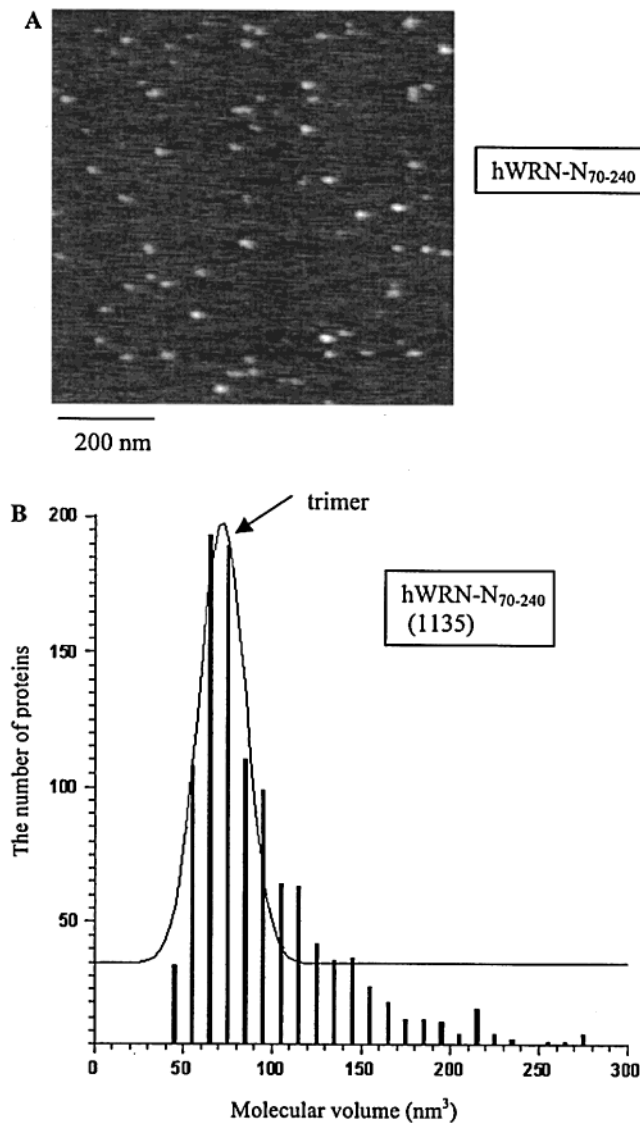
FIGURE 4: (A) AFM image of hWRN-N$_{70-240}$ at 20 nM. The image shows proper surface coverage for volume analysis. hWRN-N$_{70-240}$ was equilibrated at 37 °C for 15 min in 20 mM Tris-HCl (pH 7.8), 30 mM NaCl, 5 mM MgCl$_2$, and 5% glycerol. A deposition time of 30 s was used for this concentration of hWRN-N$_{70-240}$. The scale bar represents 200 nm. (B) Gaussian fit of the volume histogram for hWRN-N$_{70-240}$ (20 nM). The solid line is the Gaussian fit of the volume data for trimers. The number of proteins under each curve represents the population of that species. The number in parentheses (1135) represents the number of proteins that were analyzed. Only the trimer distribution has a Gaussian shape, and the fraction of trimers determined by counting the number of proteins under the curve is 83%.

FIGURE 5: Gaussian fit of the volume histogram for yeast PCNA (yPCNA) and yPCNA−hWRN-N$_{70-240}$ complexes. (A) yPCNA (40 nM) alone was equilibrated at 37 °C for 15 min in 20 mM Tris-HCl (pH 7.8), 30 mM NaCl, 5 mM MgCl$_2$, and 5% glycerol and deposited onto freshly cleaved mica for 30 s. The solid line is a Gaussian fit of the volume data for yPCNA trimers. (B) yPCNA and hWRN-N$_{70-240}$ binding in the same buffer as yPCNA alone for 15 min at room temperature prior to deposition on mica. Two distributions represent trimer yPCNA−trimer hWRN-N$_{70-240}$ complexes and trimer yPCNA−hexamer hWRN-N$_{70-240}$ complexes.

not present (Figure 4B). Because the size of the small DNA substrate S can be neglected in AFM images, we thus conclude that hWRN-N$_{70-240}$ efficiently hexamerizes in the presence of DNA.

We next sought to visualize directly complexes of hWRN-N$_{70-240}$ and DNA. A longer DNA substrate L (1 kb) was used which contained a recessed 3′-end formed by a 100-base 5′-overhang (Table 1). This DNA substrate was visualized alone by AFM and revealed molecules between 305 and 315 nm in length, as expected (Figure 6C). Upon addition of hWRN-N$_{70-240}$, it is possible to visualize hWRN-N$_{70-240}$ complexes associating with one end of this DNA substrate (Figure 6D). On the basis of the activity studies
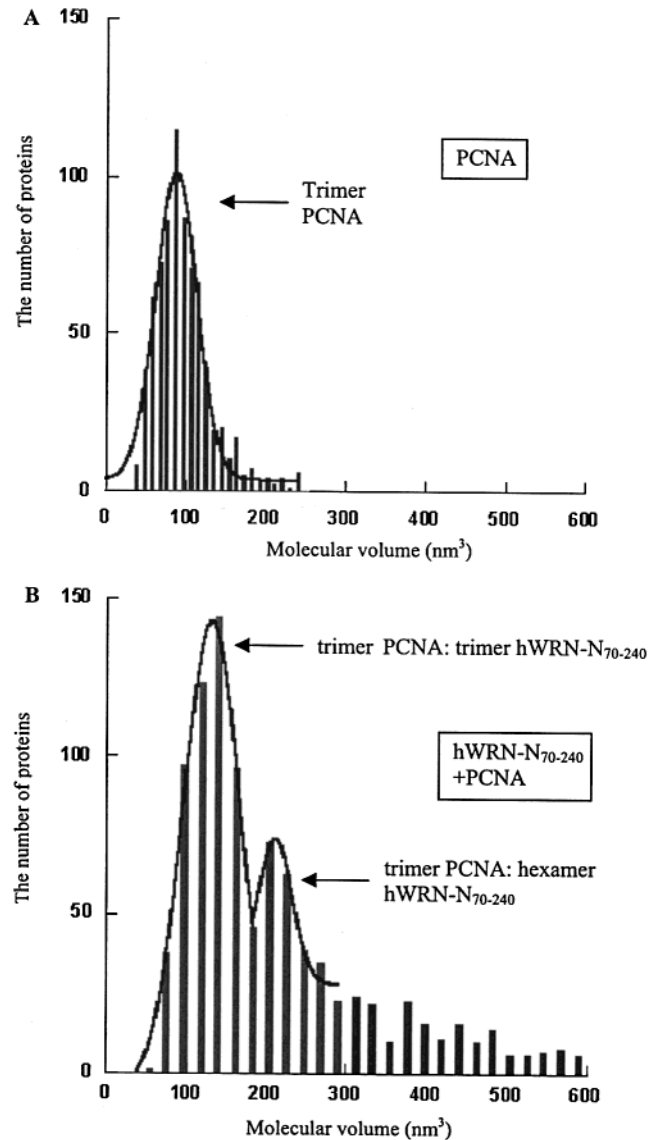
presented above, we conclude that hWRN-N$_{70-240}$ is associating with the recessed 3′-end of the DNA substrate.

These AFM studies also revealed an unexpected observation: upon incubation of hWRN-N$_{70-240}$ with the 1 kb DNA substrate L for 15 min with 1 mM ATP, we visualized the accumulation of smaller DNA fragments (e.g., Figure 6E,F). These are not the product of efficient 3′−5′ exonuclease activity by hWRN-N$_{70-240}$, as that would produce DNA molecules with single-stranded DNA ends that would still appear to be long as assessed by AFM (*35*). The observed fragments ranged in length from ~300 nm to as small as 37 nm (roughly 900 and 110 bp, respectively), with intermediate sizes such as 141 and 91 nm (430 and 275 bp, respectively) also present. We hypothesized these smaller DNA fragments
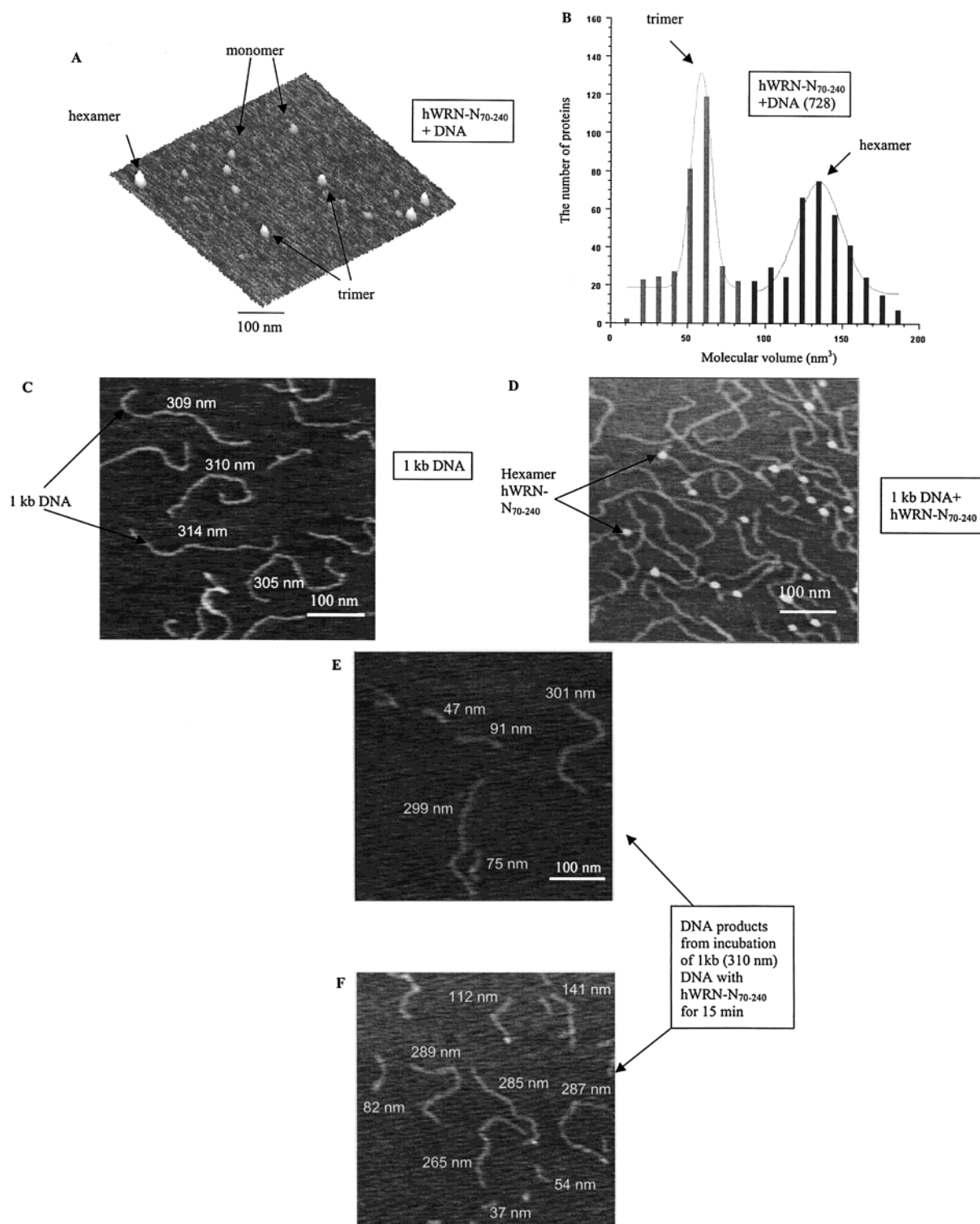
FIGURE 6: Binding of hWRN-N$_{70-240}$ to DNA containing a 3′-recessed end. (A) Surface plot of an enlarged AFM image of hWRN-N$_{70-240}$−DNA complexes. The scale bar represents 100 nm. The DNA substrate S alone is too small to be visualized by AFM (20-mer−46-mer; 7 nm in length). Arrows denote hWRN-N$_{70-240}$ monomers, trimers, and hexamers. (B) Gaussian fit of the volume histogram for hWRN-N$_{70-240}$−DNA complexes. The solid line is the Gaussian fit of the volume data for trimers and hexamers. The number of proteins under the trimer curve is 328, and the number under the hexamer curve is 360. The number in parentheses (728) is the number of total proteins that were analyzed. Both the trimer and hexamer distributions have Gaussian shapes. The fraction of trimers is 45%, and that of hexamers is 49%. The predominant hexamer peak is missing in the absence of DNA (see Figure 4). (C) AFM image of the 1 kb DNA substrate L with a 100-base 5′-overhang alone. These molecules measure between 305 and 314 nm in length, the expected length of a 900 bp DNA duplex assuming 0.33 nm per bp. (D) AFM image of hWRN-N$_{70-240}$−DNA complexes formed on the 1 kb substrate L. Bound hWRN-N$_{70-240}$ molecules can be seen at one end of several of the DNA duplexes. Volume analysis indicated that bound hWRN-N$_{70-240}$ molecules are hexamers. (E and F) AFM images of small DNA fragments generated by the digestion of DNA substrate L by hWRN-N$_{70-240}$. hWRN-N$_{70-240}$ and substrate L were incubated at 37 °C for 15 min in 1 mM ATP before deposition on mica. In panel E, DNA molecules of 301 (912 bp), 299 (906 bp), 91 (275 bp), 75 (227 bp), and 47 nm (142 bp) can been seen. In panel F, DNA molecules of 289−285 (~870 bp), 265 (803 bp), 141 (427 bp), 112 (340 bp), 82 (248 bp), 54 (163 bp), and 37 nm (112 bp) can been seen. The scale for both panels E and F is identical.
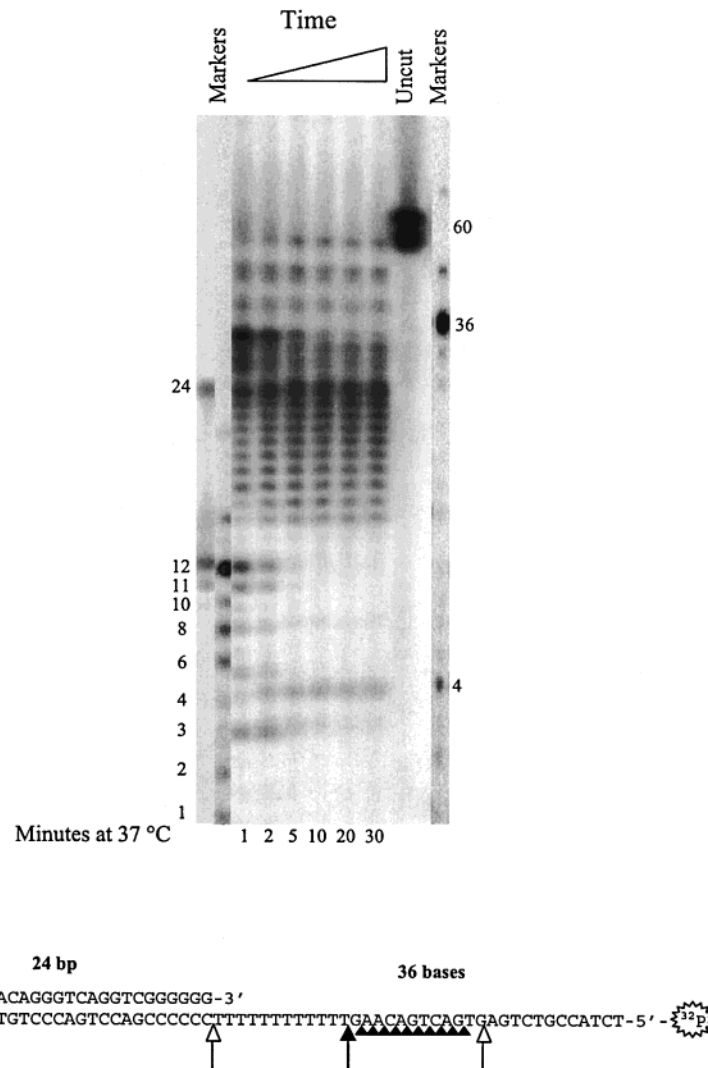
FIGURE 7: hWRN-N$_{70-240}$ endonuclease and exonuclease activities on a 5′-protruding DNA strand. The times below each lane indicate the length of time DNA substrate R, which was radiolabeled on the 5′-end of the bottom 60-nucleotide strand, and hWRN-N$_{70-240}$ were incubated together at 37 °C prior to the addition of 0.5 mM EDTA and 80% formamide. The nucleolytically fragmented ^{32}P-5′-labeled 60-mer was resolved from undigested DNA by electrophoresis through a 20% denaturing polyacrylamide gel as described (see Materials and Methods). The lane marked "uncut" contains DNA that has not been treated with hWRN-N$_{70-240}$; the position of the 5′-labeled 60-mer is indicated. Three "marker" lanes are also present, which contain standards 36, 24, 12, 10, 8, 6, 4, 3, 2, and 1 nucleotides in length. The sequence of the DNA substrate R employed in these studies is shown; this substrate contains a 24 bp duplex region and a 36-nucleotide 5′-protruding strand. The sites of the initial bursts of endonuclease cleavage that generate the 36- and 12-base products are indicated (empty arrows). The position of the nontransient endonuclease cleavage that generates the 24-base product is shown (filled arrow). In addition, the sites of 3′−5′ exonuclease cleavage of the 24-base product, the clearest single-stranded DNA exonuclease activity present in this gel, are also indicated (filled arrowheads).

were the product of a novel, protruding-strand endonuclease activity associated with hWRN-N$_{70-240}$. This activity would involve the cleavage of the intact DNA strand opposite from the recessed 3′-end. A more detailed examination of this activity is described below.

hWRN-N$_{70-240}$ Exhibits a 5′-Protruding Strand DNA Endonuclease Activity. Because AFM images of hWRN-N$_{70-240}$ incubated with DNA substrate L reveal the accumulation of smaller DNA fragments (Figure 6E,F), we suspected that hWRN-N$_{70-240}$ contained a novel nuclease activity. As stated above, we hypothesized that these smaller fragments were the product of the cleavage of the intact DNA strand opposite from the 3′-recessed DNA strand in substrate L. To examine the effect of hWRN-N$_{70-240}$ on a 5′-overhang in a DNA substrate, we employed the same substrate examined in the studies presented in Figure 2, but radiolabeled the 5′-end of

the 60-mer, rather than the 5′-end of the 24-mer (Table 1; unlabeled 24-mer/5′-^{32}P-labeled 60-mer). As shown in Figure 7, hWRN-N$_{70-240}$ was found to exhibit endonuclease activity at three sites within this substrate. First, a burst of cleavage appears to occur at two sites: at the single-strand−double-strand DNA junction, which generates the 36-base product, and within the single-stranded region of the 5′-protruding strand, which generates the 12-base product. Second, a cleavage occurs in the single-stranded, 5′-overhang region at the T$_{12}$−GAAC junction; this generates the 24-base product. The enzyme also appears to function as a 3′−5′ exonuclease on the single-stranded DNA products. This effect is most obvious in the degradation of the 24-base product to generate a ladder of smaller products, although it can also be seen in the transient degradation of the 36-base and 12-base products. It is possible that the 24-base product is generated not from

an endonuclease cleavage but from the 36-base product by efficient $3'-5'$ exonuclease action through the T_{12} region which then slows when it reaches the non-poly-T sequence. Products intermediate in length between 36 and 24 nucleotides are evident in the early time points in Figure 7. In summary, hWRN-N$_{70-240}$ contains an $5'$-protruding strand endonuclease activity at a single-strand−double-strand DNA junction and within the single-stranded region of the $5'$-protruding strand. hWRN-N$_{70-240}$ also appears to contain a $3'-5'$ exonuclease activity on the single-stranded DNA products generated from its endonuclease action. The functional implications of these additional activities are discussed below.

DISCUSSION

In our examination of a 171-amino acid exonuclease fragment of the WRN helicase/exonuclease (hWRN-N$_{70-240}$), we have found that this small construct contains $3'-5'$ exonuclease activity (Figure 2), and forms a hexamer in the presence of DNA (Figure 6). We have further shown that hWRN-N$_{70-240}$ is able to cleave a $5'$-protruding strand at the single-strand−double-strand DNA junction and within the single-stranded region of the DNA. The biological importance of the hexamer formation and these additional nuclease activities of hWRN-N$_{70-240}$ are discussed below.

A 333-amino acid N-terminal fragment of the WRN protein containing the exonuclease region was thought be a trimer based on examinations by gel filtration chromatography (*5*). We similarly found that our minimized, 171-amino acid region of the WRN exonuclease (hWRN-N$_{70-240}$) appears to be a trimer as determined by gel filtration (Figure 3). An analysis of hWRN-N$_{70-240}$ by atomic force microscopy, however, revealed that hWRN-N$_{70-240}$ is in a trimer−hexamer equilibrium in the absence of DNA with the trimer being the major species (Figure 4). We further found using AFM that the oligomerization state of hWRN-N$_{70-240}$ is dramatically shifted toward hexamers in the presence of a small DNA substrate S (Table 1 and Figure 6A,B). In addition, we visualized directly hWRN-N$_{70-240}$ hexamers bound to one end of a 1 kb piece of DNA (Figure 6D). These observations suggest that the active form of hWRN-N$_{70-240}$, and by extension the exonuclease region of full-length WRN, is a hexamer rather than a trimer.

WRN represents the first example of an exonuclease that is a hexamer. The 226-amino acid $5'-3'$ exonuclease from lambda phage, which participates in phage recombination and double-strand break repair, is a trimer in the X-ray crystal structure (*41*). This toroidal structure was determined in the absence of DNA, but was proposed to wrap around a DNA substrate to facilitate highly processive exonucleolytic cleavage of DNA. The WRN exonuclease region may exist as an analogous toroidal trimer in the absence of DNA, and these toroidal trimers may stack to form a WRN exonuclease hexamer in the presence of DNA. Alternatively, the WRN exonuclease hexamer may form a toroid, with the trimeric form of the protein existing as a half-toroid structure.

The oligomerization state of the full-length WRN protein is unknown. On the basis of its similarity to the BLM protein, which is hexameric (*42*), WRN may form a hexamer. Indeed, one critical difference between WRN and BLM is the presence of the exonuclease region in WRN, which may

impact the oligomerization state of WRN. However, the WRN exonuclease region alone appears to form a hexamer, an observation which supports the suggestion that full-length WRN is a hexamer. Such a conclusion is further supported by the finding that the interaction of hWRN-N$_{70-240}$ with PCNA appears to drive the formation of hWRN-N$_{70-240}$ hexamers (Figure 5). PCNA is composed of a trimer of pseudodimers, which together form a toroid ring (*43*). The observation that interactions with PCNA drive the formation of hWRN-N$_{70-240}$ hexamers suggests that the hWRN-N$_{70-240}$ hexamer structure may be a single toroid composed of two half-toroidal trimers, and that the hWRN-N$_{70-240}$ and PCNA toroids stack. The formation of WRN exonuclease hexamers on PCNA may in turn stabilize the hexameric form of the full-length WRN protein as well.

In examining the interaction of hWRN-N$_{70-240}$ with the 1 kb DNA substrate L by AFM, we noted smaller DNA fragments with no evidence of long single-stranded ends (Figure 6E,F). Double-stranded DNA products near 1 kb in size (e.g., 900 bp) were observed, as well as products between 430 and 110 bp in length. On the basis of these observations, we sought to determine if the WRN exonuclease region is able to cleave the $5'$-protruding strand near a single-strand−double-strand DNA junction. We found that hWRN-N$_{70-240}$ is capable of cleaving such a $5'$-protruding strand at the single-strand−double-strand DNA junction, as well as within the single-stranded region of the $5'$-protruding strand (Figure 7). In addition, it appeared that hWRN-N$_{70-240}$ further degraded these single-stranded DNA products using its $3'-5'$ exonuclease activity (Figure 7). Thus, the activities of hWRN-N$_{70-240}$ can be expanded to include not only a $3'-5'$ exonuclease acting on the recessed $3'$-end of duplex DNA but also a $5'$-protruding strand endonuclease activity and a $3'-5'$ exonuclease activity on single-stranded DNA.

In previously published reports, it was shown that full-length hWRN can cleave a one-nucleotide $5'$-flap imbedded within a DNA duplex; these authors further showed that the interaction of hWRN with the flap endonuclease Fen1 stimulates Fen1's ability to act on an identical substrate containing a $5'$-flap (*58*). In addition, it was recently shown that the interaction of the Ku 70/80 heterodimer with a construct of hWRN encompassing residues 1−388 stimulates this hWRN fragment to degrade single-stranded DNA with a $3'-5'$ polarity (*50*). Thus, human WRN appears to harbor the ability to perform multiple nuclease actions depending on the DNA substrate and hWRN's interaction with other proteins. Ku is known to interact with residues 1−50 of hWRN (*50*). Perhaps this interaction changes the positioning of these first 50 amino acids of hWRN, expanding the capabilities of the nuclease region of hWRN to include both endonuclease and exonuclease actions on single-stranded DNA. It is possible we were able to detect this activity without the presence of the Ku heterodimer because hWRN-N$_{70-240}$ lacks these first 50 amino acids. These first 50 amino acids of hWRN may serve as a regulatory region that controls the nuclease action of the enzyme.

The protruding strand endonuclease function of hWRN suggests an interesting new similarity with the Mre11 nuclease. Mre11 forms a complex with the Nbs1 and Rad50 proteins, and this complex plays important roles in DNA double-strand break repair and meiotic recombination in eukaryotes (*44−46*). Mre11 is a $3'-5'$ exonuclease in the

absence of ATP; upon addition of ATP, however, Mre11 is stimulated to cleave the 3′-protruding strand at a DNA single-strand−double-strand junction (*47*). WRN is also a 3′−5′ exonuclease and cleaves a protruding strand near a DNA single-strand−double-strand junction; in contrast to Mre11, however, WRN cleaves a 5′-protruding strand rather than a 3′-protruding strand. Parallel biological roles for WRN and the Mre11 complex have been suggested previously because genetic experiments indicate the Mre11 complex is required for efficient end joining in *S. cerevisiae* double-strand break repair (*48*). In addition, WRN has been implicated in the mammalian end-joining pathway through its association with the Ku 70/80 heterodimer (*21, 22, 49, 50*). Ku 70/80 initiates end joining in eukaryotes by binding to double-strand DNA breaks (*51*). Mre11 is thought to facilitate the joining of double-strand breaks by removing noncomplementary over-hangs or damaged bases at broken ends by its ability to combine exonuclease and endonuclease activities (*47*). Perhaps WRN's largely analogous activities allow it to substitute for Mre11 in this process in human cells. Alternatively, WRN's opposite polarity in protruding strand cleavage (5′ vs 3′ for Mre11) suggests that WRN may be called upon to cleave 5′-overhangs to generate double-strand DNA breaks, which can then be processed by the Ku heterodimer and the Mre11 complex.

WRN has also been proposed to function in DNA replication, and its physical interaction with PCNA supports this role (*5*). The identification of a 5′-protruding strand endonuclease activity associated with the WRN exonuclease region suggests a specific role for WRN in DNA replication. During lagging strand synthesis, regions of Okazaki frag-ments are displaced by a helicase and the 5′-protruding ends are cleaved by the flap endonuclease Fen1 (*52*). DNA ligase I seals the nicks remaining at the final stages of lagging strand synthesis (*53*). Both Fen1 and DNA ligase I are also known to interact physically with PCNA (*54−57*); in addition, as stated above, Fen1 and WRN are known to interact via the helicase region of WRN, and this interaction stimulates Fen1's 5′-flap endonuclease activity (*58*). WRN may be capable of combining a Fen1-like nuclease activity with a helicase function, thereby efficiently coupling these two activities during removal of Okazaki fragments. The WRN helicase region could break Watson−Crick base pairs, and the 5′-protruding endonuclease activity of the WRN exonuclease region could cleave the resulting flap. Thus, WRN may be capable of acting in concert with or substitut-ing for Fen1 and other proteins in lagging strand synthesis under particular conditions within the cell.

In summary, our results indicate that the active form of the WRN exonuclease is a hexamer, and that the interaction of the WRN exonuclease region with PCNA aids in the formation of WRN exonuclease hexamers. The formation of WRN exonuclease hexamers may be linked to, or may be the consequence of, the formation of full-length WRN protein hexamers. We have further found that the WRN exonuclease region exhibits a 5′-protruding strand endonu-clease activity. Finally, we propose that the function of WRN in human cells may be to substitute for or aid other helicases and nucleases in the processes of DNA replica-tion and/or double-strand break repair. The action of WRN as an important "backup" system in DNA replication and repair might provide one explanation for why the symptoms

of WS develop over decades, rather than being temporally acute.

REFERENCES

1. Goto, M. (1997) *Mech. Ageing Dev. 98*, 239−254.
2. Martin, G. M., Oshima, J., Gray, M. D., and Poot, M. (1999) *J. Am. Geriatr. Soc. 47*, 1136−1144.
3. Fujiwara, Y., Higashikawa, T., and Tatsumi, M. (1977) *J. Cell. Physiol. 92*, 365−374.
4. Fukuchi, K., Martin, G. M., and Monnat, R. J. (1989) *Proc. Natl. Acad. Sci. U.S.A. 86*, 5893−5897.
5. Huang, S., Beresten, S., Li, B., Oshima, J., Ellis, N. A., and Campisi, J. (2000) *Nucleic Acids Res. 28*, 2396−2405.
6. Kamath-Loeb, A. S., Shen, J. C., Loeb, L. A., and Fry, M. (1998) *J. Biol. Chem. 273*, 34145−34150.
7. Poot, M., Hoehn, H., Runger, T. M., and Martin, G. M. (1992) *Exp. Cell Res. 202*, 267−273.
8. Salk, D., Au, K., Hoehn, H., and Martin, G. M. (1981) *Cytogenet. Cell Genet. 30*, 92−107.
9. Schulz, V. P., Zakian, V. A., Ogburn, C. E., McKay, J., Jarzebowicz, A. A., Edland, S. D., and Martin, G. M. (1996) *Hum. Genet. 97*, 750−754.
10. Tahara, H., Tokutake, Y., Maeda, S., Kataoka, H., Watanabe, T., Satoh, M., Matsumoto, T., Sugawara, M., Ide, T., Goto, M., Furuichi, Y., and Sugimoto, M. (1997) *Oncogene 15*, 1911−1920.
11. Gray, M. D., Shen, J. C., Kamath-Loeb, A. S., Blank, A., Sopher, B. L., Martin, G. M., Oshima, J., and Loeb, L. A. (1997) *Nat. Genet. 17*, 100−103.
12. Huang, S., Li, B., Gray, M. D., Oshima, J., Mian, I. S., and Campisi, J. (1998) *Nat. Genet. 20*, 114−116.
13. Shen, J. C., Gray, M. D., Oshima, J., Kamath-Loeb, A. S., Fry, M., and Loeb, L. A. (1998a) *J. Biol. Chem. 273*, 34139−34144.
14. Suzuki, N., Shimamoto, A., Imamura, O., Kuromitsu, J., Kitao, S., Goto, M., and Furuichi, Y. (1997) *Nucleic Acids Res. 25*, 2973−2978.
15. Yu, C. E., Oshima, J., Fu, Y. H., Wijsman, E. M., Hisama, F., Alisch, R., Matthews, S., Nakura, J., Miki, T., Ouais, S., Martin, G. M., Mulligan, J., and Schellenberg, G. D. (1996) *Science 272*, 258−262.
16. Ellis, N. A., Groden, J., Ye, T. Z., Straughen, J., Lennon, D. J., Ciocci, S., Proytcheva, M., and German, J. (1995) *Cell 83*, 655−666.
17. Gangloff, S., McDonald, J. P., Bendixen, C., Arthur, L., and Rothstein, R. (1994) *Mol. Cell. Biol. 14*, 8391−8398.
18. Nakayama, K., Irino, N., and Nakayama, H. (1985) *Mol. Gen. Genet. 200*, 266−271.
19. Stewart, E., Chapman, C. R., Al-Khodairy, F., Carr, A. M., and Enoch, T. (1997) *EMBO J. 16*, 2682−2692.
20. Watt, P. M., Louis, E. J., Borts, R. H., and Hickson, I. D. (1995) *Cell 81*, 253−260.
21. Cooper, M. P., Machwe, A., Orren, D. K., Brosh, R. M., Ramsden, D., and Bohr, V. A. (2000) *Genes Dev. 14*, 907−912.
22. Orren, D. K., Machwe, A., Karmakar, P., Piotrowski, J., Cooper, M. P., and Bohr, V. A. (2001) *Nucleic Acids Res. 29*, 1926−1934.
23. Moser, M. J., Holley, W. R., Chatterjee, A., and Mian, I. S. (1997) *Nucleic Acids Res. 25*, 5110−5118.

24. Takeuchi, F., Hanaoka, F., Goto, M., Akaoka, I., Hori, T., Yamada, M., and Miyamoto, T. (1982) *Hum. Genet. 60*, 365−368.

25. Shen, J. C., and Loeb, L. A. (2000) *Trends Genet. 16*, 213−220.

26. Lebel, M., Spillare, E. A., Harris, C. C., and Leder, P. (1999) *J. Biol. Chem. 274*, 37795−37799.

27. Blander, G., Kipnis, J., Leal, J. F., Yu, C. E., Schellenberg, G. D., and Oren, M. (1999) *J. Biol. Chem. 274*, 29463−29469.

28. Brosh, R. M., Jr., Orren, D. K., Nehlin, J. O., Ravn, P. H., Kenny, M. K., Machwe, A., and Bohr, V. A. (1999) *J. Biol. Chem. 274*, 18341−18350.

29. Shen, J. C., Gray, M. D., Oshima, J., and Loeb, L. A. (1998) *Nucleic Acids Res. 26*, 2879−2885.

30. Blander, G., Zalle, N., Leal, J. F., Bar-Or, R. L., Yu, C. E., and Oren, M. (2000) *FASEB J. 14*, 2138−2140.

31. Duno, M., Thomsen, B., Westergaard, O., Krejci, L., and Bendixen, C. (2000) *Mol. Gen. Genet. 264*, 89−97.

32. Pichierri, P., Franchitto, A., Mosesso, P., and Palitti, F. (2000) *Mutat. Res. 456*, 45−57.

33. Poot, M., Gollahon, K. A., and Rabinovitch, P. S. (1999) *Hum. Genet. 104*, 10−14.

34. Chaconas, G., and Van de Sande, J. H. (1980) *Methods Enzymol. 65*, 75−88.

35. Ratcliff, G. C., and Erie, D. A. (2001) *J. Am. Chem. Soc. 123*, 5632−5635.

36. Gulbis, J. M., Kelman, Z., Hurwitz, J., O'Donnell, M., and Kuriyan, J. (1996) *Cell 87*, 297−306.

37. Erie, D. A., Yang, G., Schultz, H. C., and Bustamante, C. (1994) *Science 266*, 1562−1566.

38. Kasas, S., Thomson, N. H., Smith, B. L., Hansma, H. G., Zhu, X., Guthold, M., Bustamante, C., Kool, E. T., Kashlev, M., and Hansma, P. K. (1997) *Biochemistry 36*, 461−468.

39. Wyman, C., Rombel, I., North, A. K., Bustamante, C., and Kustu, S. (1997) *Science 275*, 1658−1661.

40. Wyman, C., Grotkopp, E., Bustamante, C., and Nelson, H. C. (1995) *EMBO J. 14*, 117−123.

41. Kovall, R., and Matthews, B. W. (1997) *Science 277*, 1824−1827.

42. Karow, J. K., Newman, R. H., Freemont, P. S., and Hickson, I. D. (1999) *Curr. Biol. 9*, 597−600.

43. Gulbis, J. M., Kelman, Z., Hurwitz, J., O'Donnell, M., and Kuriyan, J (1996) *Cell 87*, 297−306.

44. Haber, J. E. (1998) *Cell 95*, 583−586.

45. Mirzoeva, O. K., and Petrini, J. H. (2001) *Mol. Cell. Biol. 21*, 281−288.

46. Carney, J. P., Maser, R. S., Olivares, H., Davis, E. M., Le Beau, M., Yates, J. R., III, Hays, L., Morgan, W. F., and Petrini, J. H. (1998) *Cell 93*, 477−486.

47. Paull, T. T., and Gellert, M. (1999) *Genes Dev. 13*, 1276−1288.

48. Schiestl, R. H., and Peters, T. D. (1991) *Proc. Natl. Acad. Sci. U.S.A. 88*, 7585−7589.

49. Li, B., and Comai, L. (2000) *J. Biol. Chem. 275*, 28349−82352.

50. Li, B., and Comai, L. (2001) *J. Biol. Chem. 275*, 9896−9902.

51. Liber, M. R. (1999) *Genes Cells 4*, 77−85.

52. Li, X., Li, J., Harrington, J., Lieber, M. R., and Burgers, P. M. (1995) *J. Biol. Chem. 27*, 22109−22112.

53. Levin, D. S., Mckenna, A. E., Motycka, T. A., Matsumoto, Y., and Tomkinson, A. E. (2000) *Curr. Biol. 10*, 919−922.

54. Warbrick, E., Lane, D. P., Glover, D. M., and Cox, L. S. (1997) *Oncogene 14*, 2313−2321.

55. Li, X., Li, J., Harrington, J., Lieber, M. R., and Burgers, P. M. (1995) *J. Biol. Chem. 27*, 22109−22112.

56. Chen, V., Chen, S., Saha, P., and Dutta, A. (1996) *Proc. Natl. Acad. Sci. U.S.A. 93*, 11597−11602.

57. Levins, D. S., Bai, W., Yao, N., O'Donnell, M., and Tomkinson, A. E. (1997) *Proc. Natl. Acad. Sci. U.S.A. 94*, 12863−12868.

58. Brosh, R. M., von Kobbe, C., Sommers, J. A., Karmakar, P., Opresko, P. L., Piotrowski, J., Dianova, I., Dianov, G. L., and Bohr, V. A. (2001) *EMBO J. 20*, 5791−5801.